This Accepted Manuscript has not been copyedited and formatted. The final version may differ from this version.

eNeuro

Research Article: New Research | Neuronal Excitability

Sodium Channel-Dependent and -Independent Mechanisms Underlying Axonal Afterdepolarization at Mouse Hippocampal Mossy Fibers

Shunsuke Ohura[1] and Haruyuki Kamiya[1]

[1]*Department of Neurobiology, Hokkaido University Graduate School of Medicine, Sapporo 060-8638, Japan*

DOI: 10.1523/ENEURO.0254-18.2018

Received: 29 June 2018

Revised: 25 July 2018

Accepted: 26 July 2018

Published: 9 August 2018

Author contributions: H.K. designed the experiments. S.O. performed the experiments. H.K. performed the numerical simulation. S.O. and H.K. performed data analysis. H.K. wrote the manuscript. All the authors approved the final version of the manuscript.

Funding: http://doi.org/10.13039/501100001691Japan Society for the Promotion of Science (JSPS) KAKENHI 18K06514

Conflict of Interest: The authors report no conflict of interest.

This work was supported by JSPS KAKENHI grant number 16K15177 to HK.

Correspondence should be addressed to Haruyuki Kamiya, MD, PhD, Department of Neurobiology, Hokkaido University Graduate School of Medicine, Sapporo, 060-8638, Japan. Phone: 81-11-706-5027; Fax: 81-11-706-7863; E-mail: kamiya@med.hokudai.ac.jp

Cite as: eNeuro 2018; 10.1523/ENEURO.0254-18.2018

Alerts: Sign up at eneuro.org/alerts to receive customized email alerts when the fully formatted version of this article is published.

Accepted manuscripts are peer-reviewed but have not been through the copyediting, formatting, or proofreading process.

Copyright © 2018 Ohura and Kamiya
This is an open-access article distributed under the terms of the Creative Commons Attribution 4.0 International license, which permits unrestricted use, distribution and reproduction in any medium provided that the original work is properly attributed.

eNeuro Accepted Manuscript

eNeuro Accepted Manuscript

Sodium channel-dependent and -independent mechanisms underlying axonal afterdepolarization at mouse hippocampal mossy fibers

Shunsuke Ohura[1] and Haruyuki Kamiya[1]

[1]*Department of Neurobiology, Hokkaido University Graduate School of Medicine, Sapporo, 060-8638, Japan*

Abbreviated title:

Components of afterdepolarization in axon terminal

Correspondence should be addressed to:

Haruyuki Kamiya, M.D., Ph.D.

Department of Neurobiology, Hokkaido University Graduate School of Medicine, Sapporo, 060-8638, Japan

Phone: 81-11-706-5027

Fax: 81-11-706-7863

E-mail: kamiya@med.hokudai.ac.jp

eNeuro Accepted Manuscript

Number of Figures: 6 Figures

Number of Tables: 0 Table

Number of Multimedia: 0 multimedia

Number of words in Abstract: 250 words

Number of words in Significance statement: 117 words

Number of words in Introduction: 623 words

Number of words in Discussion: 1522 words

Acknowledgements:

This work was supported by JSPS KAKENHI grant number 16K15177 to HK.

Conflict of interest: The authors report no conflict of interest

Author contributions:

H.K. designed the experiments. S.O. performed the experiments. H.K. performed the numerical simulation. S.O. and H.K. performed data analysis. H.K. wrote the manuscript. All the authors approved the final version of the manuscript.

eNeuro Accepted Manuscript

Abstract

Action potentials propagating along axons are often followed by prolonged afterdepolarization (ADP) lasting for several tens of milliseconds. Axonal ADP is thought to be an important factor in modulating the fidelity of spike propagation during repetitive firings. However, the mechanism as well as the functional significance of axonal ADP remain unclear, partly due to inaccessibility to small structures of axon for direct electrophysiological recordings. Here, we examined the ionic and electrical mechanisms underlying axonal ADP using whole-bouton recording from mossy fiber terminals in mice hippocampal slices. ADP following axonal action potentials was strongly enhanced by focal application of veratridine, an inhibitor of Na^+ channel inactivation. On the contrary, tetrodotoxin (TTX) partly suppressed ADP, suggesting that a Na^+ channel-dependent component is involved in axonal ADP. The remaining TTX-resistant Na^+ channel-independent component represents slow capacitive discharge reflecting the shape and electrical properties of the axonal membrane. We also addressed the functional impact of axonal ADP on presynaptic function. In paired-pulse stimuli, we found that axonal ADP minimally affected the peak height of

eNeuro Accepted Manuscript

55 subsequent action potentials, although the rising phase of action potentials
56 was slightly slowed, possibly due to steady-state inactivation of Na^+ channels
57 by prolonged depolarization. Voltage clamp analysis of Ca^{2+} current elicited
58 by action potential waveform commands revealed that axonal ADP assists
59 short-term facilitation of Ca^{2+} entry into the presynaptic terminals. Taken
60 together, axonal ADP maintains reliable firing during repetitive stimuli and
61 plays important roles in the fine-tuning of short-term plasticity of
62 transmitter release by modulating Ca^{2+} entry into presynaptic terminals.
63

64 **Significance statement**

65 Axonal action potentials are often followed by depolarizing or
66 hyperpolarizing afterpotentials. This study illuminated the mechanisms of
67 ADP in the hippocampal mossy fibers, where morphological as well as
68 biophysical data were accumulated. We found that slow activating Na^+
69 channels are partly involved in ADP. Capacitive components also
70 substantially contribute to ADP, suggesting that axonal shape and electrical
71 properties are optimized for high-fidelity propagation during repetitive
72 stimuli. We also tested the roles of ADP in the activity-dependent tuning of

eNeuro Accepted Manuscript

the presynaptic Ca^{2+} current. Action potential-driven Ca^{2+} entry into the axon terminals was facilitated by paired stimuli, possibly due to Ca^{2+} current facilitation by ADP. Therefore, ADP contributes to fine-tuning of transmitter release and ensures high-fidelity spiking of axons.

eNeuro Accepted Manuscript

Introduction

The propagation of action potentials along axons is a fundamental process in the nervous system to reliably carry neuronal information to the target cells (Debanne et al., 2011; Kole and Stuart, 2012). Mechanisms enabling ultrafast and reliable spike signaling were studied extensively in various preparations of the central nervous system, including myelinated and unmyelinated axons. However, the mechanisms and functional consequences of axonal ADP, which often follows axonal action potentials and lasts for several tens of milliseconds, remain to be elucidated. Thus far, few studies have directly addressed the mechanisms for the generation of axonal ADP in the central nervous system, except for the calyx of Held axon terminals (Borst et al., 1995; Kim et al., 2010), which enable direct electrophysiological recording from the large axon terminals.

As local application of the Na^+ channel blocker tetrodotoxin (TTX) minimally affected ADP recorded from the calyx of Held axon terminals, the slow capacitive discharge of axonal membrane has been implicated in the generation of axonal ADP (Borst et al., 1995), as suggested in a previous

eNeuro Accepted Manuscript

study on lizard myelinated motor axons using intra-axonal recordings (Barrett and Barrett, 1982).

In this context, it should be noted that ADP has been demonstrated to exhibit clear dependency on the initial membrane potentials. Upon depolarization of the axonal membrane, the amplitude of ADP decreased and occasionally reversed in polarity (Begum et al., 2016; Sierksma and Borst, 2017). This indicated that ADP not only consists of passive component, but also incorporates some active component due to the activation of voltage-dependent conductance.

On the other hand, ADP was found to be largely suppressed by the application of low-concentration TTX to the same calyx of Held axon terminals (Kim et al., 2010). In this report, the author raised the possibility that certain subtypes of voltage-dependent Na^+ channels mediate ADP. Na^+ channels are functionally classified into at least three distinct subtypes: the transient-type (I_{NaT}), persistent-type (I_{NaP}), and resurgent-type (I_{NaR}). Involvement of slowly activating resurgent Na^+ current (I_{NaR}) in axonal ADP was suggested in the study by Kim et al. (2010) because dialysis of a small peptide fragment of the β4 subunit of Na^+ channels, which is an essential

eNeuro Accepted Manuscript

113 molecular component for I_{NaR}, selectively enhanced ADP. As the reason for
114 the controversial conclusion of these studies (Borst et al., 1995; Kim et al.,
115 2010) remains unclear, thorough investigation is needed to clarify the
116 mechanisms underlying axonal ADP in the central nervous system.

117 The functional significance of axonal ADP must also be addressed. It was
118 widely considered that ADP lowers the threshold of subsequent action
119 potentials, thereby enhancing the fidelity of spiking during high frequency
120 neuronal activity (Barrett and Barrett, 1982). Moreover, the prolonged time
121 course of ADP was suggested to improve fine-tuning of presynaptic functions,
122 such as action potential-driven Ca^{2+} entry and subsequent transmitter
123 release, by affecting the voltage-dependent conductance shaping axonal
124 action potentials such as Na^+ and K^+ channels. However, detailed analysis of
125 the axon terminals of calyx of Held revealed that ADP minimally affects Ca^{2+}
126 currents by balancing and cancelling out changes in the driving force and
127 gating of voltage-dependent Ca^{2+} channels (Clarke et al., 2016).

128 In this study, we examined the mechanisms underlying axonal ADP at
129 hippocampal mossy fibers, where it was reported that prominent ADP
130 follows axonal action potentials (Geiger and Jonas, 2000). Whole-cell

eNeuro Accepted Manuscript

131 recording from large axon terminals of hippocampal mossy fibers in
132 combination with numerical simulation based on a realistic model of
133 hippocampal mossy fibers (Engel and Jonas, 2005) was adopted to examine
134 the ionic and electrical mechanisms underlying axonal ADP. We also closely
135 investigated the influence of axonal ADP on action potential waveforms and
136 Ca^{2+} current in presynaptic terminals in order to evaluate its functions for
137 the activity-dependent tuning of presynaptic Ca^{2+} entry and subsequent
138 transmitter release.
139
140
141 **Materials and Methods**
142
143 **Animals and slice preparations**
144 C57BL/6J mice of either sex were used in this study, and were treated
145 according to the guidelines for the care and use of laboratory animals of
146 Hokkaido University. Transverse hippocampal slices of 300 μm thickness
147 were prepared from p14-29 mice (number of animals = 46) as described
148 previously (Kamiya, 2012; Ohura and Kamiya, 2018). Animals were

eNeuro Accepted Manuscript

anesthetized with ether, and the brain was dissected in an ice-cold sucrose solution containing the following: 40 mM NaCl, 25 mM $NaHCO_3$, 10 mM glucose, 150 mM sucrose, 4 mM KCl, 1.25 mM NaH_2PO_4, 0.5 mM $CaCl_2$, and 7 mM $MgCl_2$. Transverse slices were cut using a VT1200S microslicer (Leica Biosystems, Germany). The slices were then exchanged in a NMDG-HEPES recovery solution containing the following: 93 mM NMDG, 2.5 mM KCl, 1.2 mM NaH_2PO_4, 30 mM $NaHCO_3$, 20 mM HEPES, 25 mM glucose, 5 mM Na-ascorbate, 2 mM Thiourea, 3 mM Na-pyruvate, 10 mM $MgSO_4$, and 0.5 mM $CaCl_2$, and incubated for no longer than 15 min at 30-32°C (Ting et al., 2014). Then the solution was exchanged with standard artificial cerebro-spinal fluid (ACSF) containing the following: 127 mM NaCl, 1.5 mM KCl, 1.2 mM KH_2PO_4, 26 mM $NaHCO_3$, 10 mM glucose, 2.4 mM $CaCl_2$, and 1.3 mM $MgSO_4$, and the slices were kept in an interface-type chamber saturated with 95% O_2, and 5% CO_2. The slices were incubated in the ACSF at room temperature for at least 1 hr before experiments.

Electrophysiology

Mossy fiber boutons (MFBs) were visually identified under a microscope

eNeuro Accepted Manuscript

with IR-DIC optics (BX-51 WI, Olympus, Tokyo, Japan), as reported previously (Ohura and Kamiya, 2018; see also Geiger and Jonas, 2000; Alle and Geiger, 2006). Slices were continuously perfused at approximately 2 ml/min with ACSF. In addition, the slice surface of the recording site was locally perfused with the drug-containing solution at approximately 0.2 ml/min though a flow pipe with a 250-µm open-tip diameter connected to an electromagnetic valve system (Valve Bank, Automate Scientific, Barkley, CA). All recordings were made at room temperature (25 ± 1°C) with a patch clamp amplifier (MultiClamp700B, Molecular Devices, Sunnyvale, CA). Patch pipettes (typically 8-14 MΩ electrode resistance) were made from borosilicate glass with a microelectrode puller (Sutter P-97, Sutter Instruments, Novato, CA). Ca^{2+}-free ACSF (an equal concentration of Mg^{2+} was replaced for Ca^{2+}; 0 mM $CaCl_2$ and 3.7 mM $MgSO_4$) was perfused in the bath and focally applied to minimize the synaptic input from the surrounding cells. In whole-cell current clamp recordings, the patch pipettes were filled with an intracellular solution containing the following: 140 mM K-gluconate, 10 mM KCl, 0.2 mM EGTA, 2 mM MgATP, and 10 mM HEPES, adjusted to pH 7.2. Electrical stimuli for 200 µs were given every 10 s at the granule cell layer of the

eNeuro Accepted Manuscript

dentate gyrus, except for in experiments shown in Fig. 3*E-I*, in which stimuli were delivered every 30 s. The liquid junction potential was estimated as -15 mV using pCLAMP10 software and compensated for the holding potential. The series resistance and electrode capacitance were compensated before measurement. The recordings were adopted only when the resting membrane potentials were between -60 and -85 mV immediately after the break-in. The membrane potential was set to -80 mV manually by applying a small holding current if necessary (Geiger and Jonas, 2000). Input resistance was continuously monitored by injecting a hyperpolarizing current pulse (-10 pA, 300 ms) in each sweep. MFBs with input resistance larger than 800 MΩ and series resistance lower than 70 MΩ were used for later analyses. The data were excluded if the series resistance changed by more than 20% of the initial value during the recording. In voltage-clamp experiments, pipettes were filled with an internal solution containing the following: 145 mM CsCl, 2 mM $MgCl_2$, 2 mM Na_2ATP, 0.3 mM NaGTP, 5 mM Na_2-phosphocreatinine, 10 mM HEPES, and 10 mM EGTA, adjusted to pH 7.2. To record the Ca^{2+} current, ACSF containing 1 μM tetrodotoxin (TTX), 20 mM tetraethylammonium chloride (TEA), and 5 mM 4-aminopyridine (4AP) was

eNeuro Accepted Manuscript

203 focally applied to the recording sites. To adjust the osmolarity of the solution,
204 the concentration of NaCl in the ACSF was lowered by 20 mM. Leakage and
205 capacitive currents were subtracted online using P/4 procedures. Series
206 resistance (57.2 ± 3.3 MΩ, n = 7) was compensated by 50-70%. In some
207 recordings, unclamped tail currents with a very slow time course appeared in
208 an all-or-none manner, possibly reflecting spiking of the neighboring axons
209 or boutons. These recordings with a time constant longer than 400 μs were
210 excluded from analysis. Signals were filtered at 10 kHz with a 4-pole Bessel
211 filter, and were digitized at 20 kHz with a DIGIDATA 1322A interface and
212 16-bit resolution (Molecular Devices, Sunnyvale, CA). All data were acquired
213 and analyzed offline with pClamp 10.7 software (Molecular Devices,
214 Sunnyvale, CA) and Origin 8J or 2015 (OriginLab, Northampton, MA).
215
216 **Simulation**
217 The simulated membrane potential (V_m) at the hippocampal mossy fibers
218 was calculated according to the model suggested by Engel and Jonas (2005)
219 based on the data recorded from mossy fiber boutons. The model basically
220 assumed a Hodgkin-Huxley-type model (Hodgkin and Huxley, 1952) adapted

eNeuro Accepted Manuscript

221 to channels in mossy fiber terminals, and K^+ channels inactivation was
222 implemented multiplicatively with parameters of recombinant $K_V1.4$
223 channels (Wissmann et al., 2003). Simulations were performed using
224 NEURON 7.5 for Windows (Hines and Carnevale, 1997). The passive
225 electrical properties of the axon were assumed to be uniform, with a specific
226 membrane capacitance Cm of 1 μF $cm^{-2,}$ a specific membrane resistance Rm
227 of 10,000 Ω cm^2, and an intracellular resistivity Ri of 110 Ω cm. The
228 structure of the mossy fiber was approximated by a soma (diameter, 10 μm),
229 10 axonal cylinders (diameter, 0.2 μm; length, 100 μm), and 10 *en passant*
230 boutons (diameter, 4 μm). The number of segments was 1 μm^{-1}, and the time
231 step was 5 μs in all simulations. The resting potential was assumed to be −80
232 mV. The reversal potential of the leak conductance was set to −81 mV to
233 maintain stability. Voltage-gated Na^+ channels, K^+ channels, and leakage
234 channels were inserted into the soma, axon, and boutons, respectively. The
235 Na^+ conductance density was set to 50 mS cm^{-2} for the axon and boutons,
236 and 10 mS cm^{-2} for the soma. The K^+ conductance density was set to 36 mS
237 cm^{-2} throughout all parts of the neurons. Action potentials were evoked by
238 injection of depolarizing current into the 9th bouton (1 ms, 0.15 nA) or the

eNeuro Accepted Manuscript

239 soma (2 ms, 0.2 nA) in the simulation shown in Fig. 4*G* and 4*H*, respectively.
240 We carried out stimulation on the last (10th) bouton in a "pearl chain
241 structure" to avoid sealed end effects. The equilibrium potentials for Na^+ and
242 K^+ ions were assumed to be +50 mV and −85 mV, respectively.
243
244 **Statistics**
245 All data are expressed as the mean ± SEM. Statistical analysis was
246 performed by non-parametric two-sided tests (Wilcoxon signed-rank test for
247 paired data and Mann-Whitney U test for unpaired data), and a *P* value of <
248 0.05 was accepted for statistical significance. All statistical analyses were
249 carried out using R software (version 3.4.1).
250
251 **Chemicals**
252 Veratridine was purchased from Sigma-Aldrich (St. Louis, MO, USA).
253 Tetrodotoxin was purchased from Funakoshi (Tokyo, Japan). All other
254 chemicals were purchased from Wako Pure Chemical (Tokyo, Japan).

eNeuro Accepted Manuscript

Results

Slow ADP following axonal action potentials at hippocampal mossy fibers

To characterize the detailed properties of ADP following action potentials, whole-cell current clamp recordings were made from large MFBs in mouse hippocampal slices (Fig. 1*A*). Long depolarizing current pulses (20-120 pA, 500 ms) in the current clamp configuration constantly evoked single action potentials to increasing currents (Fig. 1*B*), as reported previously (Geiger and Jonas, 2000; Bischofberger et al., 2006). Input resistance and the time constant of MFBs were also measured from voltage responses to hyperpolarizing current injection of -10 pA for 300 ms. Input resistance and the decay time constant were 1.06 ± 0.06 GΩ and 36.4 ± 3.3 ms, respectively (n = 20), and were consistent with those reported in previous studies (Bischofberger et al., 2006; Szabadics and Soltesz, 2009). Action potentials were also evoked by extracellular stimulation at the granule cell layer of the dentate gyrus (Fig. 1*C*, left). The amplitude and half-width of action potentials evoked by stimulation of granule cells were 114.5 ± 2.4 mV and 863 ± 34 μs, respectively (n = 20). Alternatively, injection of short current

eNeuro Accepted Manuscript

pulses (500-800 pA for 1 ms) to the recorded bouton also elicited action potentials (Fig. 1*C*, right). The amplitude and half-width of the action potentials evoked by current injection were 113.8 ± 2.6 mV and 918 ± 26 μs, respectively (n = 6), which were not significantly different from those evoked by stimulation at the granule cell layer (P = 0.700 and P = 0.422 for amplitude and half duration, respectively).

In each stimulation mode of input stimulation or current injection, a small and prolonged ADP followed the action potentials in MFBs (Geiger and Jonas, 2000; Kamiya et al., 2002), as shown in Fig. 1*C* (arrowheads). The amplitude and decay time constant of ADP by stimulation of input fibers were 15.3 ± 1.3 mV and 41.6 ± 3.8 ms, respectively (n = 20), which were not significantly different from those evoked by current injection to the recorded boutons (13.0 ± 1.3 mV and 43.6 ± 5.5 ms), as shown in Fig. 1*D* (P = 0.494 for amplitude and P = 0.700 for decay time constant). As these data were recorded in Ca^{2+}-free ACSF to minimize the influence of synaptically released transmitters (Ohura and Kamiya, 2018), ADP was considered to have originated intrinsically from the membrane properties of MFBs.

Previous reports suggested that R-type Ca^{2+} channels contribute to ADP

eNeuro Accepted Manuscript

291 in CA1 pyramidal neurons (Metz et al., 2005), and mossy fiber terminals
292 contain R-type Ca^{2+} channels (Gasparini et al., 2001; Li et al., 2007).
293 However, any possible contribution of R-type Ca^{2+} channels to ADP
294 generation was omitted in the recording in Ca^{2+}-free solution. To test for
295 possible contribution of R-type Ca^{2+} channels in axonal ADP in the mossy
296 fibers, we examined the effects of Ca^{2+}-containing ACSF, and found no
297 significant changes in action potentials or ADP generated by short current
298 injection (P = 0.742 and P =0.742, respectively, n = 8, Fig. 1*E, F*). This
299 suggests that ADP at mossy fiber terminals was not mediated by Ca^{2+}
300 channel-dependent components.
301
302 **Voltage dependency of axonal ADP**
303 To investigate the mechanisms underlying ADP, we first examined the
304 voltage-dependency of ADP amplitude. For this purpose, membrane
305 potentials were changed by injecting continuous currents into the recording
306 MFBs. At positive membrane potentials relative to resting membrane
307 potentials, the amplitude of ADP was decreased and the waveform was
308 markedly altered (Fig. 2*A, B*). In these experiments, we measured

eNeuro Accepted Manuscript

membrane potentials at 5 ms after the peak of the action potentials because the peak of ADP was evident at that time point. The ADP amplitude was 16.7 ± 1.6 mV in the control conditions at -79.1 ± 0.6 mV, and decreased to 7.5 ± 1.1 mV at the depolarized conditions of -66.2 ± 0.9 mV (n = 14, P = 0.00012, Fig. 2*C*). The negative correlation of ADP with initial membrane potentials was also reported at presynaptic terminals of the calyx of Held (Sierksma and Borst, 2017) or cerebellar basket cells (Begum et al., 2016).

Sodium channel-dependent component of axonal ADP

It was reported that the slow reactivation of resurgent-type Na^+ currents mediates ADP at the presynaptic terminals of the calyx of Held (Kim et al., 2010). Focal application of 0.5 μM TTX to the recording site completely abolished both action potentials (from 108.9 ± 4.0 mV to 1.0 ± 0.4 mV, n = 6, P = 0.0313) and ADP (from 12.4 ± 1.2 mV to 0.4 ± 0.2 mV, n = 6, P = 0.0313), as shown in Fig. 3*A*. To test for possible contribution of Na^+ channels to ADP, we examined the effects of TTX on ADP. For this purpose, brief current pulses of 2000-4300 pA for 1 ms were injected to mimic the short depolarization of action potentials (103.7 ± 6.7 mV, n = 6) in the presence of TTX (Fig. 3*A*). The

eNeuro Accepted Manuscript

peak amplitude of ADP was decreased to 10.3 ± 1.3 mV by TTX (n = 6), and the difference in ADP amplitudes between with and without TTX was significant (P = 0.0313), as shown in Fig. 3*D*. This suggests that TTX-sensitive Na^+-channels partly mediate ADP at MFBs.

On the other hand, a previous study revealed that veratridine, an inhibitor of sodium channel inactivation, markedly enhanced and prolonged ADP at the calyx of Held presynaptic terminals (Kim et al., 2010). Therefore, we examined the effects of veratridine on action potentials and ADP at hippocampal MFBs. Application of 1 μM veratridine had minimal effects on the action potentials (Fig. 3*E, F*). The amplitude and half-width of action potentials were 107.6 ± 6.0 mV and 1.02 ± 0.03 ms, respectively, in the control conditions, whereas they were 106.0 ± 7.4 mV and 1.07 ± 0.06 ms, respectively, after application of veratridine (n = 6). The differences were not significant (P = 0.563 and 0.688, Fig. 3*G, H*). However, the amplitude of ADP was significantly increased from 10.8 ± 1.5 mV to 13.5 ± 1.9 mV by veratridine (n = 6, P = 0.0313, Fig. 3*I*). During application of veratridine for 10 min, 3 out of 6 recordings exhibited mild enhancement and prolongation of ADP, as shown in Fig. 3E, but the other 3 recordings accompanied multiple

eNeuro Accepted Manuscript

345 spikes overlaying enhanced ADP (Fig. 3*F*). These results suggest that
346 veratridine-sensitive Na^+ channels contributed to the generation of ADP,
347 although the amount varied among boutons. As ADP largely remained with
348 TTX (Fig. 3*B, D*), a mechanism other than Na^+ channels is involved in the
349 generation of ADP.
350
351 **Capacitive component of axonal ADP**
352 Next, we addressed the contribution of the component derived from slow
353 capacitive discharge of the axonal membrane (Barrett and Barrett, 1982;
354 Borst et al., 1995; David et al., 1995). As shown in Fig. 3*A*, brief current
355 injection into the MFBs elicited prolonged depolarization resistant to the
356 application of TTX. To measure the components of capacitive discharge, we
357 evaluated the effects of 4-AP, which almost completely blocks potassium
358 channels at MFBs (Alle et al., 2011), on TTX-resistant depolarization.
359 Application of 2 mM 4-AP increased the amplitude of the slow depolarization
360 component at 5 ms from 11.6 ± 0.9 mV to 26.0 ± 4.0 mV (n = 8, P=0.00781),
361 as shown in Fig. 4*A* and 4*B*. The decay time constant was also increased by
362 4-AP (from 30.9 ± 4.8 ms to 37.6 ± 6.1 ms, n = 8, P=0.00781, Fig. 4*C*). These

eNeuro Accepted Manuscript

363 results suggest that delayed activation of voltage-dependent K^+ channels
364 curtails the repolarizing phase of the brief depolarization by TTX, and the
365 voltage responses elicited in the presence of TTX and 4-AP most likely
366 represent capacitive components due to axonal membrane discharge. This
367 notion is supported by the findings that the time constant (37.6 ± 6.1 ms) was
368 not significantly different from that observed in hyperpolarization elicited by
369 stepwise negative current injection (37.7 ± 6.7 ms, n = 8) (P = 0.547, Fig. 4*F*).
370 As expected from the passive nature of capacitive discharge, the time course
371 of this component was voltage-independent (Fig. 4*E*). The amplitudes were
372 26.0 ± 4.0 mV at -80 mV and 25.3 ± 3.9 mV at -70 mV, and the difference was
373 not significant (P = 0.945). The decay time constant recorded at -80 mv (37.6
374 ± 6.1 ms) was not different from that at -70 mV (35.8 ± 6.1 ms, n = 8, P =
375 0.813).

376 To quantitatively evaluate the contribution of the capacitive component,
377 we also carried out numerical simulation using the model described
378 previously (Engel and Jonas, 2005). This was a realistic mossy fiber model
379 incorporating the compartmental cable model mimicking the morphology of
380 mossy fiber axons, as well as a Hodgkin-Huxley-type gating model of

eNeuro Accepted Manuscript

voltage-dependent Na^+ channels that was obtained experimentally and implemented with inactivation of voltage-dependent K^+ channels. Hyperpolarization evoked by negative current injection was optimally fit with the sum of two exponentials, reflecting two electrical components of boutons and the connecting axons, and the time constant of the dominant component was 17.0 ms (Fig. 4*G*, left). The decay time constant for short current injection, in which both Na^+ and K^+ conductance was reduced to 0, was 15.0 ms (Fig. 4*G*, right).

We also carried out simulation for passive propagation of the action potentials through a thin axonal cable from the nearby MFBs. For this purpose, we reconstituted the propagation of action potentials elicited by injecting stimuli at the soma, and calculated the voltage transients at the distal axons and the MFBs (Fig. 4*H*). Simulation demonstrated that the action potential of nearby MFBs (108.2 mV in amplitude) was passively propagated to the next MFBs (17.3 mV in amplitude). The spatial distribution constant of the passive propagation of transient signal, which we defined in this study as the distance that reduced the size of the transient signal to 1/e (37%) without any active conductance, was estimated as 53.6 μm,

eNeuro Accepted Manuscript

399 and this value was similar with that reported for Purkinje cell axons
400 (Zorrilla de San Martin et al., 2017). Therefore, the capacitive component of
401 ADP may reflect the propagation of action potentials at upstream axons
402 and/or MFBs.

403 In the absence of active conductance, action potentials passively
404 propagate and decay exponentially with distance. However, this spatial
405 distribution of transient voltage changes is strongly filtered by the electrical
406 cables of thin axons, and should be different from and shorter than those of
407 steady-state responses indicated by the length constant, which represents
408 the duration for decay of the size of steady-state responses to 1/e.

409 These results suggest that the decay time course of ADP is mainly
410 determined by the slow capacitive discharge of the axonal membrane
411 following action potentials. Veratridine-sensitive Na^+ channels and
412 4AP-sensitive K^+ channels additionally contribute to ADP to modulate the
413 time course in mouse hippocampal MFBs.

414

415 **Broadening of axonal action potentials by ADP**

416 Our previous study revealed short-term depression of axonal spikes, as

eNeuro Accepted Manuscript

417 recorded by loose-patch clamp recording (Ohura and Kamiya, 2018). As
418 application of veratridine selectively depressed the second spike with
419 minimal effects on the first spike, we supposed that ADP following the first
420 action potential affects the second action potential by steady-state
421 inactivation of voltage-dependent Na^+ channels. Thus, to examine the effects
422 of ADP on activity-dependent modulation of action potentials, we first
423 examined whether steady-state depolarization affects the action potentials
424 (Fig. 5*A, B*). The amplitude of the action potential was measured from the
425 baseline before stimulation because it was difficult to detect the threshold of
426 propagating action potentials due to their smooth rising phase. The small
427 depolarization preceding AP (13.4 ± 0.8 mV from control) caused no
428 significant change in the peak amplitude (to 97.7 ± 2.9% of control) or the
429 half-width of action potentials (to 97.8 ± 2.3% of control) (n = 14, P = 0.542
430 and 0.326). The latency to the onset of action potentials was shortened to
431 85.9 ± 5.7% of the control (n = 14, P = 0.00842).

432 We then examined how ADP affects the subsequent action potentials.
433 For this purpose, we recorded consecutive action potentials in response to
434 the paired-pulse stimuli at short intervals (Fig. 5*C*). The peak membrane

eNeuro Accepted Manuscript

potential was slightly reduced to 96.8 ± 1.1% of the control at a 10-ms interval (n = 8, P = 0.0173, Fig. 5*D*), but was not significantly changed at longer intervals (to 99.7 ± 0.5%, 100.0 ± 0.2%, 99.8 ± 0.2% of the control at 20-ms, 50-ms, or 100-ms intervals, respectively) (P = 1, 0.889, 0.674 for 20-ms, 50-ms, 100-ms, n = 8, Fig. 5D). The peak reduction at the 10-ms interval was possibly due to incomplete recovery from the inactivation of Na^+ channels (Engel and Jonas, 2005). We also examined the absolute value of the amplitude of action potentials. The amplitude of the second action potential was significantly reduced at 10-, 20-, and 50-ms intervals (to 86.8 ± 2.3%, 91.0 ± 1.4%, 97.2 ± 0.6% of the control, P = 0.00195, 0.000479, 0.00352, respectively), and it almost recovered to the basal level at a 100-ms interval (to 99.5 ± 0.5%, P = 0.287979), as shown in Fig. 5*D*. These time courses of depression of the second action potentials were similar with those of ADP, which lasted for several tens of ms.

We recently reported that axonal spikes recorded by loose-patch clamp recording were markedly depressed in response to paired-pulse stimuli (Ohura and Kamiya, 2018). As the derivative of action potentials was found to be proportional to the extracellularly recorded axonal spikes by the

eNeuro Accepted Manuscript

loose-patch configuration (Meeks et al., 2005; Ohura and Kamiya, 2018), we calculated the first derivative of the action potential by whole-cell recording (Fig. 5*E*). The second amplitude of the derivative of action potentials (Fig. 5*F*) was slightly lower than the first (88.4 ± 4.1%, 92.6 ± 1.5%, 96.4 ± 0.9%, 97.8 ± 0.5% of control for 10-, 20-, 50-, and 100-ms intervals, respectively). The differences were significant (P = 0.00781, 0.00781, 0.00781, 0.00781, for 10-, 20-, 50-, and 100-ms intervals, n = 8). The time course was consistent with that of axonal spikes recorded by loose-patch clamp recordig (Ohura and Kamiya, 2018).

We also examined the changes in duration of action potentials by paired stimuli. Repolarization was slightly slowed and the half-width of the action potentials was prolonged at short intervals (113 ± 5, 110 ± 2, 104 ± 1% of the control at 10-, 20-, and 50-ms intervals, P = 0.00781, 0.00781, 0.00781, respectively), but the difference was not significant at a 100-ms interval (102 ± 1% of control, P = 0.148), as shown in Fig. 5*G, H*. These findings were consistent with the previous study demonstrating activity-dependent broadening of action potentials by cumulated inactivation of potassium channels (Geiger and Jonas, 2000).

eNeuro Accepted Manuscript

471

472 **Facilitation of presynaptic Ca^{2+} current by ADP**

473 Lastly, we examined whether ADP modifies the presynaptic Ca^{2+} current,
474 which directly controls transmitter release and short-term plasticity.
475 Pharmacologically-isolated Ca^{2+} currents (Fig. 6*A*) exhibited a typical time
476 course of slow activation followed by fast tail currents, as in the previous
477 study (Bischofberger et al., 2002). The current-voltage (I-V) relationship was
478 also similar with that reported previously. Ca^{2+} currents were activated from
479 approximately -40 mV and reached a maximum amplitude of 134 ± 15 pA at
480 10 mV (n = 7), as shown in Fig. 6*B*. The voltage-dependency of the activation
481 of Ca^{2+} current was also estimated by measuring tail currents and plotted
482 against the voltage (Fig. 6*C*). The steady-state activation data were fitted by
483 a Boltzmann function with a slope factor of 10.4 mV and midpoint potential
484 of -7.0 mV. These profiles of presynaptic Ca^{2+} currents in the MFBs were
485 consistent with those reported in previous studies (Bischofberger et al., 2002;
486 Li et al., 2007).

487 To explore the influence of ADP on the presynaptic Ca^{2+} influx,
488 voltage-clamp recordings of Ca^{2+} currents were made using voltage

eNeuro Accepted Manuscript

commands mimicking the action potential waveforms recorded by paired-pulse stimuli shown in Fig. 5*C*. The charge transfer of Ca^{2+} currents was measured as the integrated area under the curve. The half-width of Ca^{2+} currents was also measured as the duration between the time points of the half and peak heights. The Ca^{2+} currents elicited by the second action potential voltage-commands with ADP at 10 ms were slightly facilitated compared with those elicited by the first action potential commands at 115.2 ± 8.5% of the control, and the half-width increased to 117.8 ± 7.7% (n = 7). These effects depended on the intervals of paired stimuli, and were abolished at a 100-ms interval (to 103.0 ± 2.7% for the charge and to 102.1 ± 0.6% for the half-width). We considered this Ca^{2+} current facilitation by paired-pulse action potentials to be due to the broadening of action potentials, as shown in Fig. 5*G*, or facilitation of Ca^{2+} channels by prolonged depolarization during ADP. To investigate these possibilities, mock action potential-like voltage commands mimicking broadening of action potential but lacking ADP were applied to measure Ca^{2+} currents for comparison (Fig. 6*D*). In these recordings, Ca^{2+} currents were not facilitated (to 91.2 ± 3.3% and 104.6 ± 2.6% for 10-ms and 100-ms intervals, respectively, n = 7). At a 10-ms interval,

eNeuro Accepted Manuscript

507 the difference in the facilitation of Ca^{2+} current between with and without
508 ADP was significant (P = 0.0156). The half-width of the Ca^{2+} current was
509 unaffected by mock action potentials with ADP (to 102.2 ± 2.8% and 102.1 ±
510 2.0% for 10 ms and 100 ms intervals, respectively, n = 7). These results
511 suggest that slight broadening of action potentials minimally affects Ca^{2+}
512 entry, but ADP itself facilitates it, possibly by a similar mechanism to those
513 recently reported at presynaptic terminals of cerebellar Purkinje cells
514 (Zorrilla de San Martin et al., 2017). Although the underlying mechanisms
515 remain to be elucidated, ADP following preceding action potentials
516 modulates Ca^{2+} entry into the presynaptic terminals by the second action
517 potential, and may affect the short-term facilitation of transmitter release.
518

eNeuro Accepted Manuscript

519 **Discussion**

520 In this study, we examined the mechanisms underlying the prominent
521 ADP following axonal action potentials using direct whole-cell recordings
522 from hippocampal mossy fiber terminals in mice. We found that the axonal
523 ADP was generated predominantly by slow capacitive discharge of the
524 axonal membrane reflecting passive propagation of action potentials. Slow
525 activating Na^+ channels also partly increase the capacitive component of the
526 axonal ADP. On the other hand, voltage-dependent K^+ channels curtail the
527 initial phase of ADP by accelerating repolarization. Furthermore, we also
528 examined the functional consequences of axonal ADP in the regulation of
529 presynaptic functions. We found that prolonged subthreshold depolarization
530 of axonal ADP facilitates the presynaptic Ca^{2+} current, thereby possibly
531 modulating short-term synaptic plasticity.

532

533 **Components of axonal ADP**

534 Action potentials recorded from the soma were often followed by ADP
535 lasting for several tens of ms, and were considered to regulate the fidelity of
536 successive neuron firing during repetitive stimuli (Schwartzkroin, 1975;

eNeuro Accepted Manuscript

537 Storm, 1987). In addition, ADP is also known to be accompanied by action
538 potentials propagating along axons. Thus far, axonal ADP was observed in
539 several preparations allowing for direct recording from the axon and
540 terminals such as in lizard motor axons (Barrett and Barrett, 1982), calyx of
541 Held axon terminals (Borst et al., 1995), and hippocampal mossy fiber
542 terminals (Geiger and Jonas, 2000). Therefore, the mechanisms of axonal
543 ADP have been studied thoroughly, but remain somewhat controversial
544 (Borst et al., 1995; Kim et al., 2010; Sierksma and Borst, 2017).

545 Regarding the mechanisms of axonal ADP, it has been widely accepted
546 that the slow capacitive discharge of propagating action potentials
547 contributes substantially to ADP (Barrett and Barrett, 1982), as expected
548 from the cable properties of axons. As focal application of TTX minimally
549 affected ADP at calyx of Held axon terminals (Borst et al., 1995), axonal ADP
550 may be caused by, at least in part, a passive component due to capacitive
551 discharge. In accordance with this notion, we found that the time course of
552 slow repolarization of capacitive components, as measured in TTX and 4-AP
553 conditions, was almost comparable to that of ADP.

554 On the other hand, ADP also demonstrated clear voltage-dependency, as

eNeuro Accepted Manuscript

555 shown in Fig. 2, which is different from the passive nature of the capacitive
556 component. Therefore, involvement of voltage-dependent conductance in the
557 generation of ADP is reasonable. In support of this notion, veratridine, which
558 has complex effects on Na^+ channels but mainly exerts its facilitating action
559 by inhibiting inactivation (Ulbricht, 1998), robustly enhanced ADP and it
560 sometimes became overlaid with multiple spikes. On the contrary, blocking
561 Na^+ channels with TTX partly reduced ADP. These results were consistent
562 with the contribution of some slowly activating voltage-dependent Na^+
563 channels to the generation of ADP, as reported in the calyx of Held axon
564 terminals (Kim et al., 2010).

565 Previous studies demonstrated that slowly activating sodium channels,
566 such as persistent-type I_{NaP} (Yue et al., 2005; D'Ascenzo et al., 2009; Kole,
567 2011; Ghitani et al., 2016) or resurgent-type I_{NaR} (Raman and Bean, 1997),
568 different from transient-type I_{NaT} responsible for generation of action
569 potentials, are involved in ADP. We previously reported that ADP in the
570 granule cell soma in the dentate gyrus, which was reported to highly express
571 I_{NaR} (Castelli et al., 2007), was markedly enhanced by veratridine (Ohura
572 and Kamiya, 2018). This implies that ADP in hippocampal mossy fiber

eNeuro Accepted Manuscript

573 terminals may also be mediated by resurgent-type I_{NaR}. Direct testing for the
574 presence of I_{NaR} in future studies will help to reveal the contribution of
575 specific Na^+ channels to ADP at hippocampal mossy fibers.

576 We also found that voltage-dependent K^+ channels sensitive to 4-AP are
577 involved in the shaping of ADP. It was previously demonstrated that
578 repolarization of action potentials at the MFBs is regulated by K_V1 (Geiger
579 and Jonas, 2000) and K_V3 (Alle et al., 2011) voltage-dependent K^+ channels.
580 K^+ currents elicited by action potential waveform commands are sensitive to
581 4-AP, and were fully suppressed at 1 mM (Alle et al., 2011). We confirmed
582 that 4-AP at 2 mM substantially delayed the repolarization of "mock" action
583 potentials elicited in the presence of TTX, and the time course of residual
584 components were voltage-independent, as shown in Fig. 4*E*. These results
585 suggest that voltage-dependent K^+ channels are also involved in the early
586 phase of ADP to shorten the prolonged depolarization. This is consistent with
587 the finding that ADP at the calyx of Held axon terminals is also negatively
588 controlled by Kv1.1/1.2-type K^+ channels to prevent multiple spikes during
589 ADP (Dodson et al., 2003). The contribution of K_V7 should be examined in a
590 future study as it was found to alter the somatic ADP in pyramidal cells (Yue

eNeuro Accepted Manuscript

591 and Yaari, 2004; Gu et al., 2005; Brown and Randall, 2009) and is present on
592 hippocampal mossy fibers (Martinello et al., 2015).

593 Taken together, we consider ADP at hippocampal mossy fibers to consist
594 of passive and active components. Passive capacitive discharge dominates
595 and determines the time course of ADP. As active components, possible slow
596 activating voltage-dependent Na^+ channels sensitive to veratridine and TTX
597 partly amplify the slow capacitive component. Voltage-dependent K^+
598 channels sensitive to 4-AP also participate in shaping the early phase of ADP
599 at hippocampal mossy fibers.

600 This interpretation may clarify the voltage-dependency of axonal ADP
601 (Fig. 2). In several previous studies, the voltage-dependency of axonal ADP
602 upon changes in membrane potentials was reported, and "apparent" reversal
603 potentials also varied between different preparations (Begum et al., 2016;
604 Sierksma and Borst, 2017). The differential contribution of capacitive
605 mechanism, as well as Na^+ and K^+ channel-dependent mechanisms, may
606 explain the complex voltage-dependency of axonal ADP. Our study clarified
607 that sodium channel-dependent and -independent mechanisms underlie ADP
608 at hippocampal mossy fibers.

eNeuro Accepted Manuscript

609

610 **Role of ADP in activity-dependent modulation of axonal action potentials**

611 The functional consequence of ADP on subsequent axonal action
612 potentials was examined thoroughly in previous studies. It was reported that
613 ADP plays pivotal roles in ensuring reliable firing upon multiple stimuli
614 (Borst et al., 1995; Kim et al., 2010), as well as in modulating firing patterns
615 (Bean, 2007; Sierksma and Borst, 2017). In this study, we examined
616 activity-dependent modulation of the action potential waveform by ADP of
617 preceding action potentials. ADP exhibited minimal effects on the peak of
618 successive action potentials, except at very short intervals of 10 ms when
619 Na^+ channels are not fully recovered from inactivation by the preceding
620 action potentials (Brody and Yue, 2000; He et al., 2002; Engel and Jonas,
621 2005). However, peaks of the calculated first derivatives of action potentials,
622 which are considered to reflect the maximal rate of the rising phase of action
623 potentials, demonstrated paired-pulse depression for up to 100 ms. This is
624 consistent with our previous observation that axonal spikes recorded
625 extracellularly using loose-patch clamp recording had paired-pulse
626 depression following a similar time course (Ohura and Kamiya, 2018)

eNeuro Accepted Manuscript

627 because extracellularly recorded axonal spikes are theoretically proportional
628 to the first derivative of action potentials (Meeks et al., 2005).
629 Furthermore, activity-dependent broadening of action potentials (Geiger
630 and Jonas, 2000) was detectable even in paired-pulse protocols in this study.
631 As suggested, accumulated inactivation of K_V1-type voltage-dependent K^+
632 channels may cause activity-dependent broadening of action potentials at
633 hippocampal mossy fibers. A similar mechanism may underlie ADP, although
634 the magnitude of broadening is much smaller.
635
636 **Role of ADP in facilitation of the presynaptic Ca^{2+} current**
637 The shape of the presynaptic action potential determines the calcium
638 influx to the presynaptic terminals, and thereby modulates transmitter
639 release from the presynaptic terminals. Broadening of action potentials
640 during repetitive stimuli was reported to enhance the calcium influx into
641 presynaptic terminals (Geiger and Jonas, 2000; Bischofberger et al., 2002).
642 Even in the paired-stimuli conditions, mild broadening of action potentials
643 was observed, but it minimally affected the Ca^{2+} current elicited by "mock"
644 action potentials without ADP, as shown in Fig. 6*D*. Although it is unclear

eNeuro Accepted Manuscript

why the Ca^{2+} current was not facilitated by paired-pulse, the positive effects of spike broadening may be counteracted or cancelled by residual inactivation of Ca^{2+} channels at short intervals. Slight changes in action potential rise times may also contribute to this apparent discrepancy.

On the other hand, Ca^{2+} currents elicited by voltage-clamp commands of the recorded action potentials with ADP were slightly but significantly facilitated. Recently, direct recording from Purkinje cell axon terminals revealed that prior subthreshold depolarization facilitated Ca^{2+} currents (Zorrilla de San Martin et al., 2017). Although the detailed biophysical mechanism awaits future investigation, a similar mechanism may underlie the paired-pulse facilitation of Ca^{2+} currents observed in this study.

Functional implications

Axonal ADP following action potentials is a fundamental and important upstream process of transmitter release, which accordingly affects short-term synaptic plasticity. In this study, we found that the axonal ADP may facilitate presynaptic Ca^{2+} currents elicited by action potentials. As it has been demonstrated that somatic depolarization also affects transmitter

eNeuro Accepted Manuscript

release from MFBs in a Ca^{2+}-independent manner (Scott et al., 2008), Ca^{2+} current facilitation as well as Ca^{2+}-independent facilitation of transmitter release may be involves in the activity-dependent short-term plasticity at synapses. Simultaneous recording from both presynaptic MFBs and postsynaptic pyramidal cells (Vyleta and Jonas, 2014; Midorikawa and Sakaba, 2017) to quantitatively correlate presynaptic Ca^{2+}-signaling with postsynaptic EPSPs will clarify the detailed functions of axonal ADP for the short-term plasticity at hippocampal mossy fiber synapses.

eNeuro Accepted Manuscript

672 **References**

673

674 Alle H, Geiger JR (2006) Combined analog and action potential coding in
675 hippocampal mossy fibers. Science 311:1290-1293.
676 Alle H, Kubota H, Geiger JR (2011) Sparse but highly efficient K_v3 outpace
677 BK_{Ca} channels in action potential repolarization at hippocampal mossy
678 fiber boutons. J Neurosci 31:8001-8012.
679 Barrett EF, Barrett JN (1982) Intracellular recording from vertebrate
680 myelinated axons: mechanism of the depolarizing afterpotential. J
681 Physiol 323:117-144.
682 Bean BP (2007) The action potential in mammalian central neurons. Nat
683 Rev Neurosci 8:451-465.
684 Begum R, Bakiri Y, Volynski KE, Kullmann DM (2016) Action potential
685 broadening in a presynaptic channelopathy. Nat Commun 7:12102.
686 Bischofberger J, Geiger JR, Jonas P. (2002) Timing and efficacy of Ca^{2+}
687 channel activation in hippocampal mossy fiber boutons. J Neurosci
688 22:10593-10602.
689 Bischofberger J, Engel D, Li L, Geiger JR, Jonas P (2006) Patch-clamp

eNeuro Accepted Manuscript

recording from mossy fiber terminals in hippocampal slices. Nat Protoc 1:2075-2078

Borst JG, Helmchen F, Sakmann B (1995) Pre- and postsynaptic whole-cell recordings in the medial nucleus of the trapezoid body of the rat. J Physiol 489:825-840.

Brody DL, Yue DT (2000) Release-independent short-term synaptic depression in cultured hippocampal neurons. J Neurosci 20:2480-2494.

Brown JT, Randall AD (2009) Activity-dependent depression of the spike after-depolarization generates long-lasting intrinsic plasticity in hippocampal CA3 pyramidal neurons. J Physiol 587:1265-1281.

Castelli L, Nigro MJ, Magistretti J (2007) Analysis of resurgent sodium-current expression in rat parahippocampal cortices and hippocampal formation. Brain Res 1163:44-55.

Clarke SG, Scarnati MS, Paradiso KG (2016) Neurotransmitter release can be stabilized by a mechanism that prevents voltage changes near the end of action potentials from affecting calcium currents. J Neurosci 36:11559-11572.

D'Ascenzo M, Podda MV, Fellin T, Azzena GB, Haydon P, Grassi C (2009)

eNeuro Accepted Manuscript

708 Activation of mGluR5 induces spike afterdepolarization and enhanced
709 excitability in medium spiny neurons of the nucleus accumbens by
710 modulating persistent Na^+ currents. J Physiol 587:3233-3250.
711 Debanne D, Campanac E, Bialowas A, Carlier E, Alcaraz G (2011) Axon
712 physiology. Physiol Rev 91:555-602.
713 David G, Modney B, Scappaticci KA, Barrett JN, Barrett EF (1995)
714 Electrical and morphological factors influencing the depolarizing
715 after-potential in rat and lizard myelinated axons. J Physiol
716 489:141-157.
717 Dodson PD, Billups B, Rusznák Z, Szûcs G, Barker MC, Forsythe ID (2003)
718 Presynaptic rat Kv1.2 channels suppress synaptic terminal
719 hyperexcitability following action potential invasion. J Physiol
720 550:27-33.
721 Engel D, Jonas P (2005) Presynaptic action potential amplification by
722 voltage-gated Na^+ channels in hippocampal mossy fiber boutons. Neuron
723 45:405-417.
724 Gasparini S, Kasyanov AM, Pietrobon D, Voronin LL, Cherubini E (2001)
725 Presynaptic R-type calcium channels contribute to fast excitatory

eNeuro Accepted Manuscript

726 synaptic transmission in the rat hippocampus. J Neurosci 21:8715-8721.

727 Geiger JR, Jonas P (2000) Dynamic control of presynaptic Ca^{2+} inflow by

728 fast-inactivating K^+ channels in hippocampal mossy fiber boutons.

729 Neuron 28:927-939.

730 Ghitani N, Bayguinov PO, Basso MA, Jackson MB (2016) A sodium

731 afterdepolarization in rat superior colliculus neurons and its

732 contribution to population activity. J Neurophysiol jn.01138.02015.

733 Gu N, Vervaeke K, Hu H, Storm JF (2005) Kv7/KCNQ/M and HCN/h, but not

734 KCa2/SK channels, contribute to the somatic medium

735 after-hyperpolarization and excitability control in CA1 hippocampal

736 pyramidal cells. J Physiol 566:689-715.

737 He Y, Zorumski CF, Mennerick S (2002) Contribution of presynaptic Na^+

738 channel inactivation to paired-pulse synaptic depression in cultured

739 hippocampal neurons. J Neurophysiol 87:925-936.

740 Hines ML, Carnevale NT (1997) The NEURON simulation environment.

741 Neural Comput 9:1179-1209.

742 Hodgkin AL, Huxley AF (1952) A quantitative description of membrane

743 current and its application to conduction and excitation in nerve. J

eNeuro Accepted Manuscript

744 Physiol 116:497-506.

745 Kamiya H, Ozawa S, Manabe T (2002) Kainate receptor-dependent

746 short-term plasticity of presynaptic Ca^{2+} influx at the hippocampal

747 mossy fiber synapses. J Neurosci 22:9237-9243.

748 Kamiya H (2012) Photochemical inactivation analysis of temporal dynamics

749 of postsynaptic native AMPA receptors in hippocampal slices. J Neurosci

750 32:6517-6524.

751 Kim JH, Kushmerick C, von Gersdorff H (2010) Presynaptic resurgent Na^{+}

752 currents sculpt the action potential waveform and increase firing

753 reliability at a CNS nerve terminal. J Neurosci 30:15479-15490.

754 Kole MH (2011) First node of Ranvier facilitates high-frequency burst

755 encoding. Neuron 71:671-682.

756 Kole MH, Stuart GJ (2012) Signal processing in the axon initial segment.

757 Neuron 73:235-247.

758 Li L, Bischofberger J, Jonas P (2007) Differential gating and recruitment of

759 P/Q-, N-, and R-type Ca^{2+} channels in hippocampal mossy fiber boutons.

760 J Neurosci 27:13420-13429.

761 Martinello K, Huang Z, Lujan R, Tran B, Watanabe M, Cooper EC, Brown

eNeuro Accepted Manuscript

762 DA, Shah MM (2015) Cholinergic afferent stimulation induces axonal
763 function plasticity in adult hippocampal granule cells. Neuron
764 85:346-363.
765 Meeks JP, Jiang X, Mennerick S (2005) Action potential fidelity during
766 normal and epileptiform activity in paired soma-axon recordings from rat
767 hippocampus. J Physiol 566:425-441.
768 Metz AE, Jarsky T, Martina M, Spruston N (2005) R-type calcium channels
769 contribute to afterdepolarization and bursting in hippocampal CA1
770 pyramidal neurons. J Neurosci 25:5763-73.
771 Midorikawa M, Sakaba T (2017) Kinetics of releasable synaptic vesicles and
772 their plastic changes at hippocampal mossy fiber synapses. Neuron
773 96:1033-1040.
774 Ohura S, Kamiya H (2018) Short-term depression of axonal spikes at the
775 mouse hippocampal mossy fibers and sodium channel-dependent
776 modulation. eNeuro 5. pii: ENEURO.0415-17.2018.
777 Raman IM, Bean BP (1997) Resurgent sodium current and action potential
778 formation in dissociated cerebellar Purkinje neurons. J Neurosci
779 17:4517-4526.

eNeuro Accepted Manuscript

780 Schwartzkroin PA (1975) Characteristics of CA1 neurons recorded
781 intracellularly in the hippocampal in vitro slice preparation. Brain Res
782 85:423-436.
783 Scott R, Ruiz A, Henneberger C, Kullmann DM, Rusakov DA (2008) Analog
784 modulation of mossy fiber transmission is uncoupled from changes in
785 presynaptic Ca^{2+}. J Neurosci 28:7765-7773.
786 Sierksma MC, Borst JGG (2017) Resistance to action potential depression of
787 a rat axon terminal in vivo. Proc Natl Acad Sci U S A 114:4249-4254.
788 Storm JF (1987) Action potential repolarization and a fast
789 after-hyperpolarization in rat hippocampal pyramidal cells. J Physiol
790 385:733-759.
791 Szabadics J, Soltesz I (2009) Functional specificity of mossy fiber innervation
792 of GABAergic cells in the hippocampus. J Neurosci 29:4239-4251.
793 Ting JT, Daigle TL, Chen Q, Feng G (2014) Acute brain slice methods for
794 adult and aging animals: application of targeted patch clamp analysis
795 and optogenetics. Methods Mol Biol 1183:221-242.
796 Ulbricht W (1998) Effects of veratridine on sodium currents and fluxes. Rev
797 Physiol Biochem Pharmacol 133:1-54.

eNeuro Accepted Manuscript

798 Vyleta NP, Jonas P (2014) Loose coupling between Ca^{2+} channels and release
799 sensors at a plastic hippocampal synapse. Science 343:665-670.
800 Wissmann R, Bildl W, Oliver D, Beyermann M, Kalbitzer HR, Bentrop D,
801 Fakler B (2003) Solution structure and function of the "tandem
802 inactivation domain" of the neuronal A-type potassium channel Kv1.4. J
803 Biol Chem 278:16142-16150.
804 Yue C, Yaari Y (2004) KCNQ/M channels control spike afterdepolarization
805 and burst generation in hippocampal neurons. J Neurosci 24:4614-4624.
806 Yue C, Remy S, Su H, Beck H, Yaari Y (2005) Proximal persistent Na+
807 channels drive spike afterdepolarizations and associated bursting in
808 adult CA1 pyramidal cells. J Neurosci 25:9704-9720.
809 Zorrilla de San Martin J, Trigo FF, Kawaguchi SY (2017) Axonal $GABA_A$
810 receptors depolarize presynaptic terminals and facilitate transmitter
811 release in cerebellar Purkinje cells. J Physiol 595:7477-7493.
812

eNeuro Accepted Manuscript

Figure Legends.

Figure 1. Prominent ADP following action potentials at MFBs in mouse hippocampal slices. ***A***, IR-DIC image of the recorded bouton (arrow) and CA3 pyramidal cell (arrowhead). Scale bar represents 5 μm. ***B***, Whole-cell recordings confirmed typical membrane potential responses of MFBs with single action potentials in response to the current injection (-20 to 120 pA pulses for 500 ms, 20 pA each step). ***C***, Action potential of MFBs evoked by input stimuli at the granule cell layer (left) and current injection at the recorded boutons (right). The arrowheads represent the peaks of ADP. ***D***, Summary data of the amplitude of ADP elicited by input stimuli (open column; n = 20) or by current injection (closed column, n = 6). ***E***, Effects of Ca^{2+}-containing ACSF on action potentials elicited by current injection. ***F***, Summary of ADP amplitude in the absence (open column) and presence (closed column) of Ca^{2+} (n = 8).

Figure 2. Dependency of ADP on initial membrane potentials. ***A***, Action potentials were recorded at control (black) and depolarized (red) membrane

eNeuro Accepted Manuscript

831 potentials by injecting constant currents into the recorded boutons. Although
832 the peak of action potentials was unaffected by changes in initial membrane
833 potentials, the amplitude and the time course of ADP were significantly
834 altered by changes in the membrane potentials. ***B***, Superimposed traces
835 illustrate the voltage-dependency of ADP. ***C***, Summary data for ADP
836 amplitude recorded at control and depolarized initial membrane potentials
837 (n = 14).
838
839 **Figure 3.** Involvement of Na^+ channels in axonal ADP. ***A***, Action potentials
840 evoked by input stimuli (black) were completely suppressed by application of
841 0.5 μM TTX (red). Large current injection into the recorded MFB elicited
842 "mock" action potentials with similar time courses of action potentials and
843 ADP (blue). ***B***, Superimposed control (black) and "mock" action potentials
844 (blue) demonstrated that TTX-sensitive components overtook the
845 TTX-resistant slow ADP, suggesting that TTX-sensitive Na^+-channels partly
846 enhance ADP. ***C, D***, Comparison of control and "mock" action potentials (**C**)
847 and ADP (***D***) amplitude (n = 6, $*P < 0.05$). ***E, F***, Effects of focal application of
848 1 μM veratridine, an inhibitor of Na^+ channel inactivation, on ADP.

eNeuro Accepted Manuscript

Veratridine enhanced and prolonged ADP (***E***). In some cases, multiple action potentials (***F***) were overlaid, as shown in the right panel. ***G***, ***H***, ***I***, Summary data for the effects of veratridine on the amplitude (***G***), half-width (***H***) of action potentials, and the amplitude of ADP (***I***) (n = 6, * $P < 0.05$).

Figure 4. Contribution of capacitive slow discharge in the axonal ADP. ***A***, "Mock" action potentials (black) elicited by large current injection into MFBs in the presence of TTX were prolonged by the addition of 2 mM 4-AP (red), leaving the capacitive components of the axonal membrane. ***B***, ***C***, Summary data for the amplitude (***B***) and decay time constant (***C***) of ADP (n = 8, * $P <$ 0.05). ***D***, Time constant of MFBs measured by hyperpolarizing current injection (-10 pA, 300 ms). ***E***, Comparison of decay time course of capacitive components at different initial membrane potentials of -80 and -70 mV. **F**, Summary data for decay time constants of hyperpolarization (***D***) and the capacitive component of ADP at -80 mV (***E***). ***G***, Simulated membrane potentials in the mossy fiber model by Engel & Jonas (2005) in response to hyperpolarizing current injection into distal MFBs (left). Brief large current injection elicited a similar response to those observed in ***A*** (right) when gNa

eNeuro Accepted Manuscript

867 and gK were omitted from the distal axons shown in red. See Methods for
868 details. ***H***, Simulation of passive propagation of upstream action potentials
869 to distal axons where gNa and gK were omitted.
870
871 **Figure 5.** Broadening of axonal action potentials by the preceding ADP. ***A***,
872 Effects of changes in initial membrane potentials on action potentials elicited
873 by stimulation of input fibers recorded at depolarized (red) or resting (black)
874 membrane potentials. ***B***, Summary data for the relative peak, half-width,
875 and latency of action potentials (n = 14). ***C***, Superimposed traces of
876 paired-pulse responses at 10-, 20-, 50-, and 100-ms intervals. ***D***, Summary
877 data for the paired-pulse ratio of action potential amplitude measured from
878 the onset of the second action potential (n = 8). ***E***, First derivatives calculated
879 from paired-pulse responses are shown in ***C*** and ***F***, Summary data for the
880 paired-pulse ratio of the first derivative waveform (n = 8). ***G***, Expanded
881 traces of the 1st (black) and 2nd (red) action potentials at different
882 inter-spike intervals. ***H***, Summary data for the paired-pulse ratio of the
883 action potential half-width (n = 8).
884

eNeuro Accepted Manuscript

885 **Figure 6.** Facilitation of presynaptic Ca^{2+} influx by the axonal ADP. ***A***, Ca^{2+}
886 currents in MFBs evoked by voltage steps from -80 mV to -70 ~ 50 mV for 20
887 ms. ***B***, The averaged I-V relationships of presynaptic Ca^{2+} currents at MFBs.
888 Current amplitudes were measured at the end of the voltage steps. ***C***,
889 Voltage-dependency of activation of Ca^{2+} currents as shown by the
890 amplitudes of tail currents. Data were normalized to the maximal value in
891 each experiment and were fitted using a Boltzmann function (n = 7). ***D***,
892 Voltage-clamp recording of Ca^{2+} currents using voltage commands mimicking
893 the action potential waveforms elicited by paired-pulse stimuli (red). For
894 comparison, "mock" action potential-like voltage commands mimicking
895 broadening of action potentials by 10% in accordance with data in Fig. 5***H***,
896 but lacking ADP, were applied (blue). Superimposed Ca^{2+} currents evoked by
897 the 1st and 2nd voltage commands are shown in the right panels. ***E***, ***F***,
898 Summary data for the paired-pulse ratio of charge transfer (***E***) and
899 half-width (***F***) of Ca^{2+} currents (n = 7, * $P < 0.05$).

eNeuro Accepted Manuscript

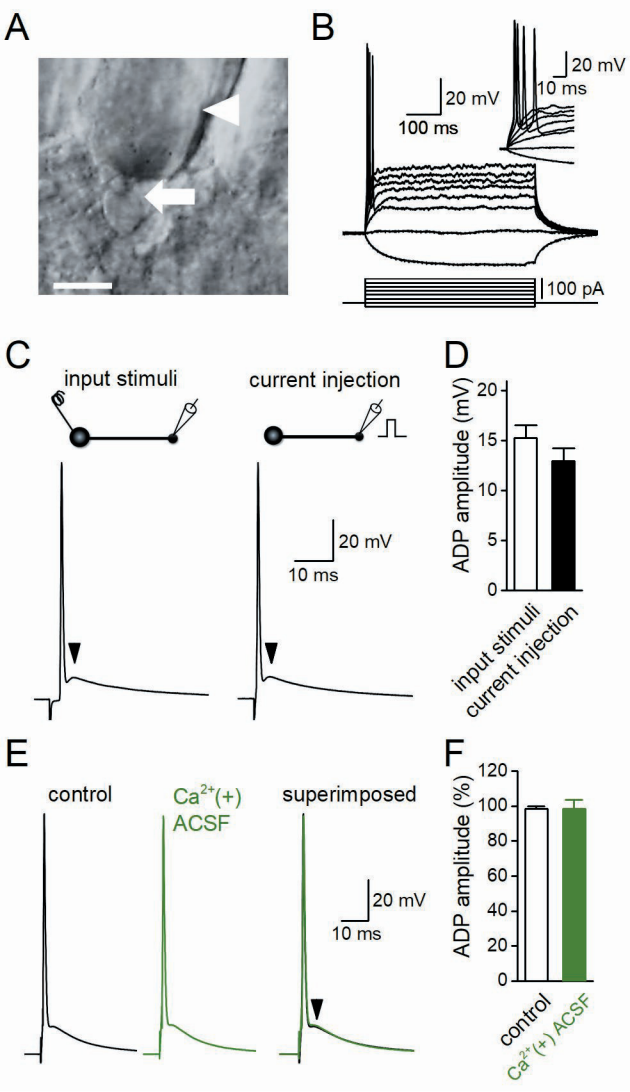

eNeuro Accepted Manuscript

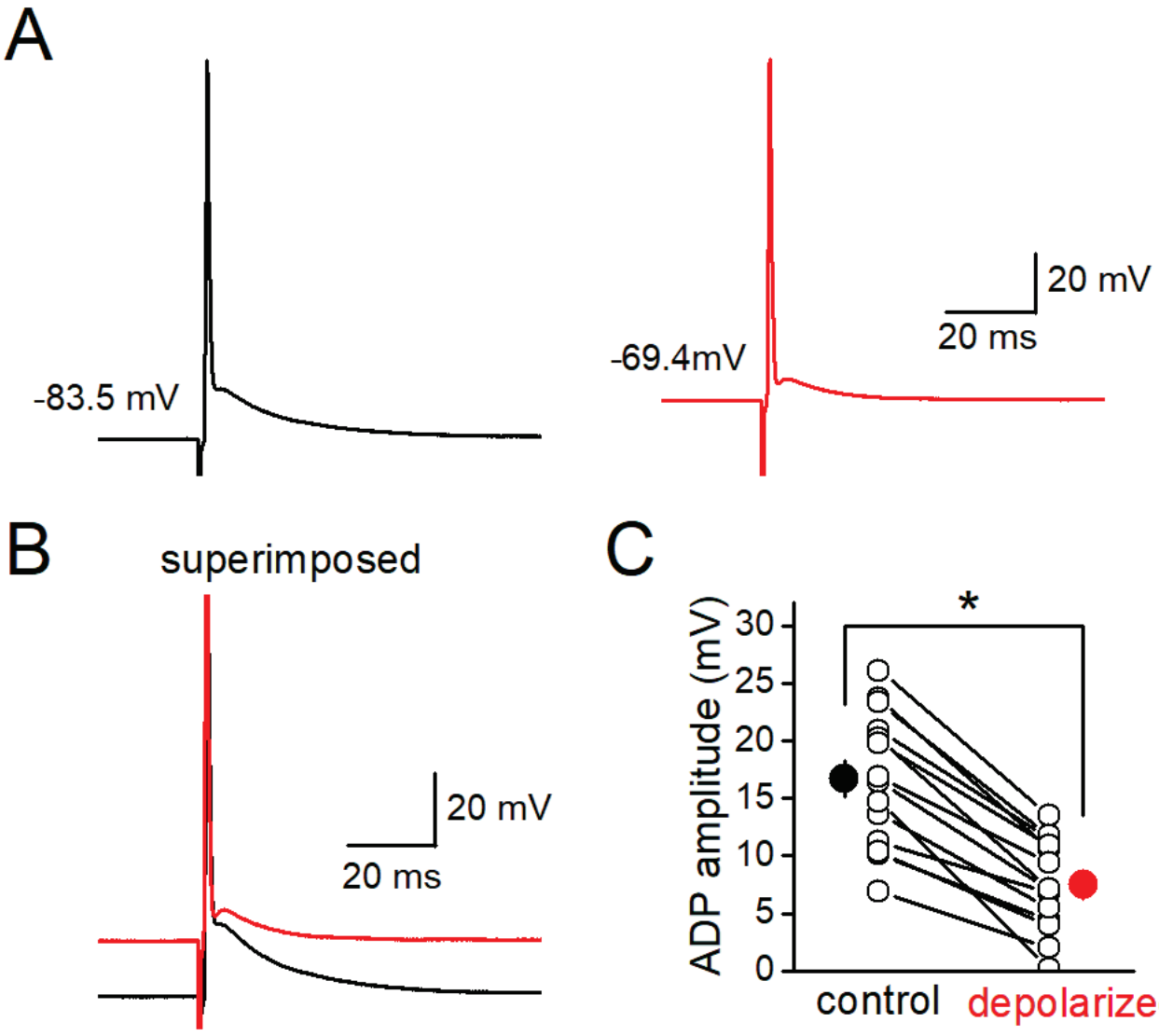

eNeuro Accepted Manuscript

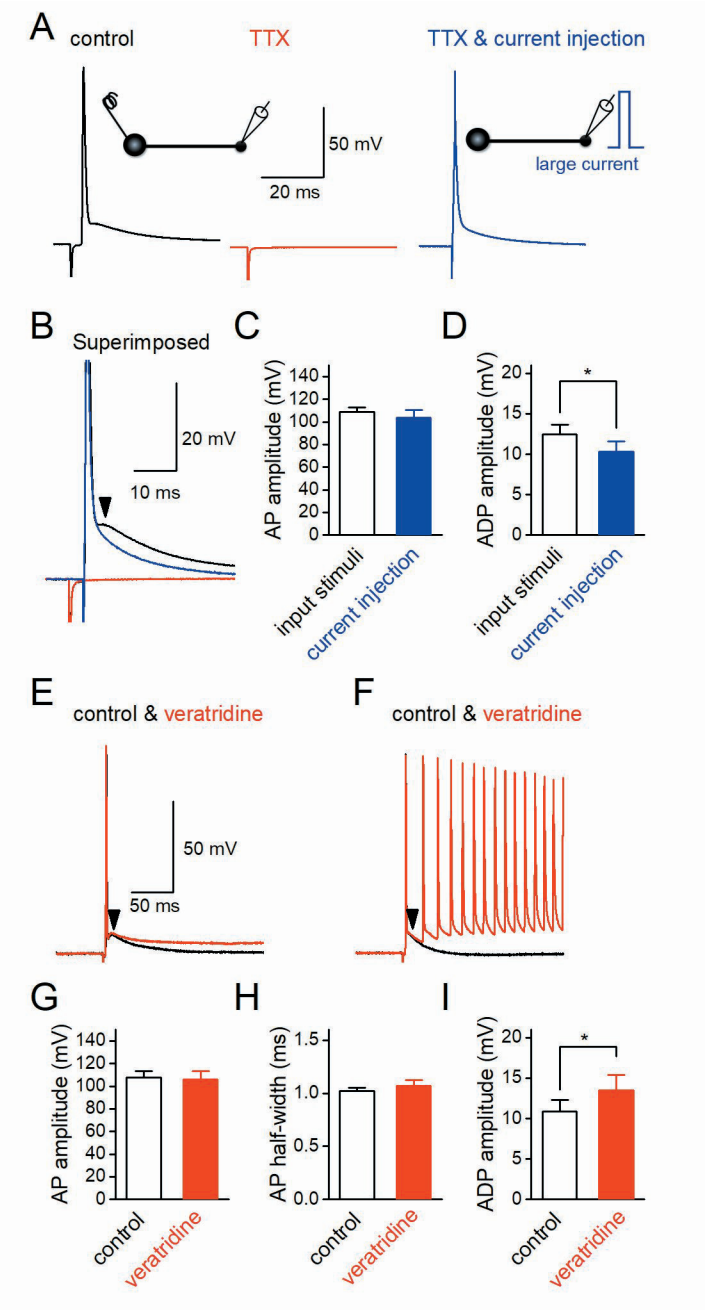

eNeuro Accepted Manuscript

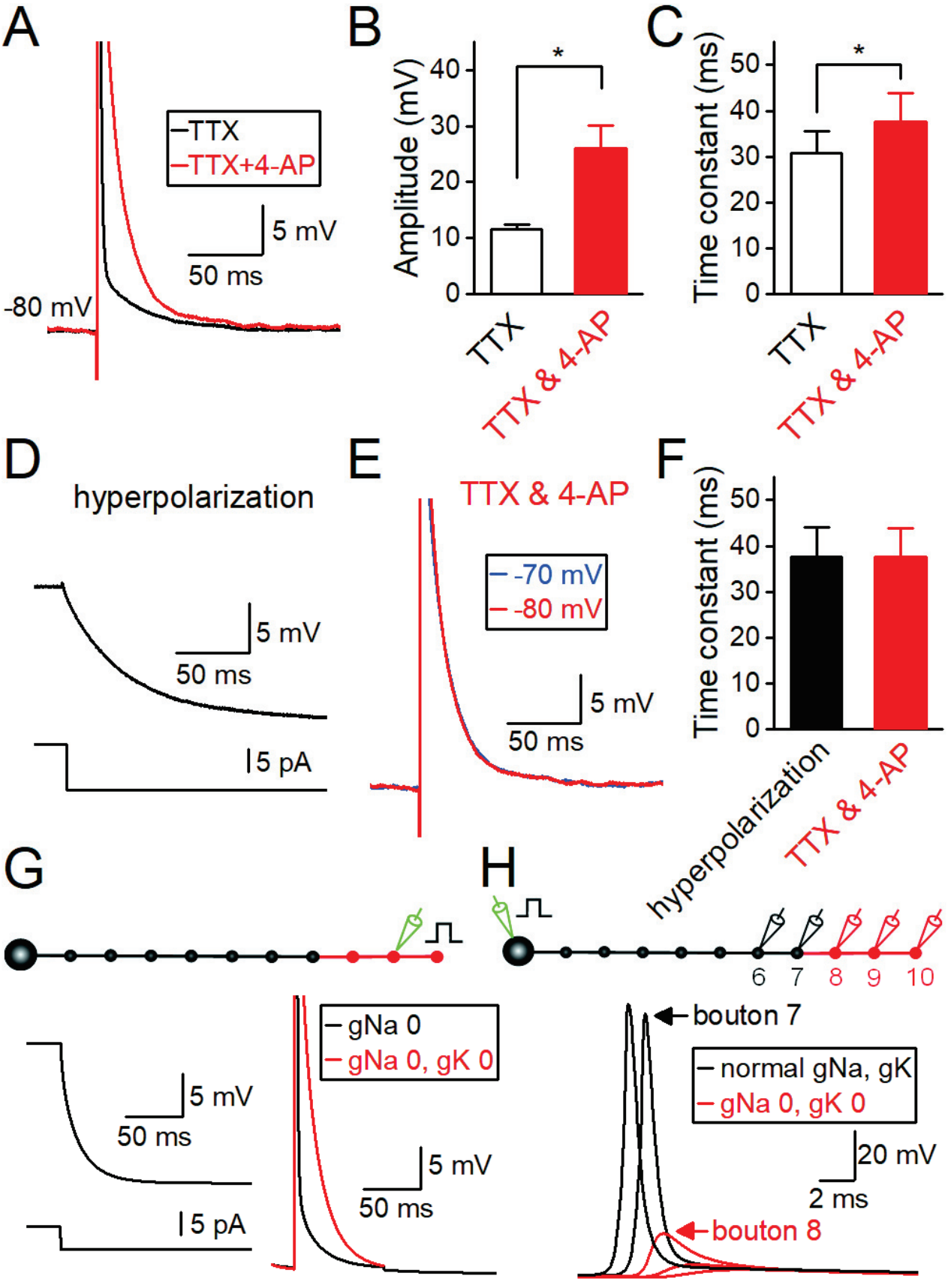

eNeuro Accepted Manuscript

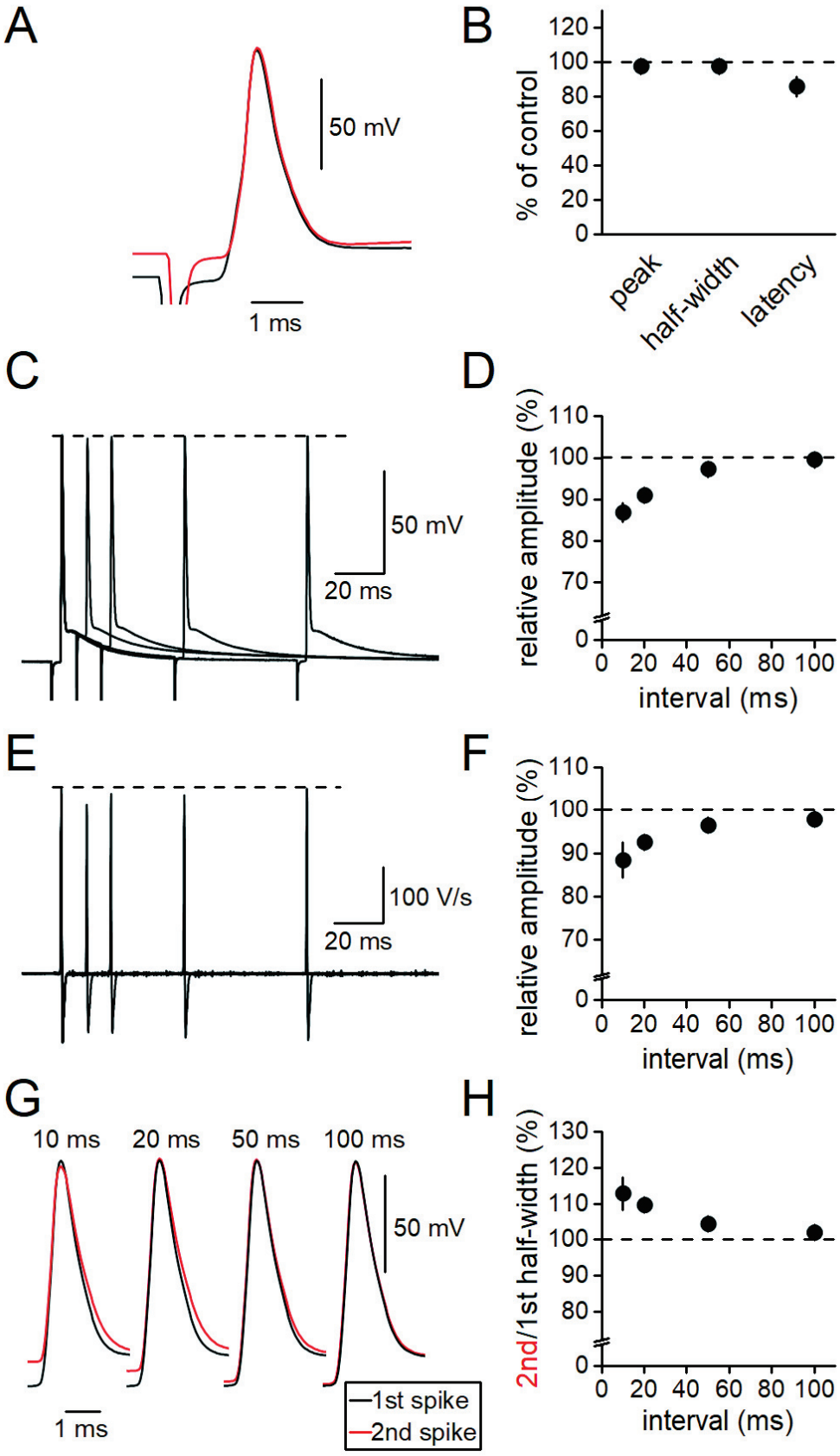
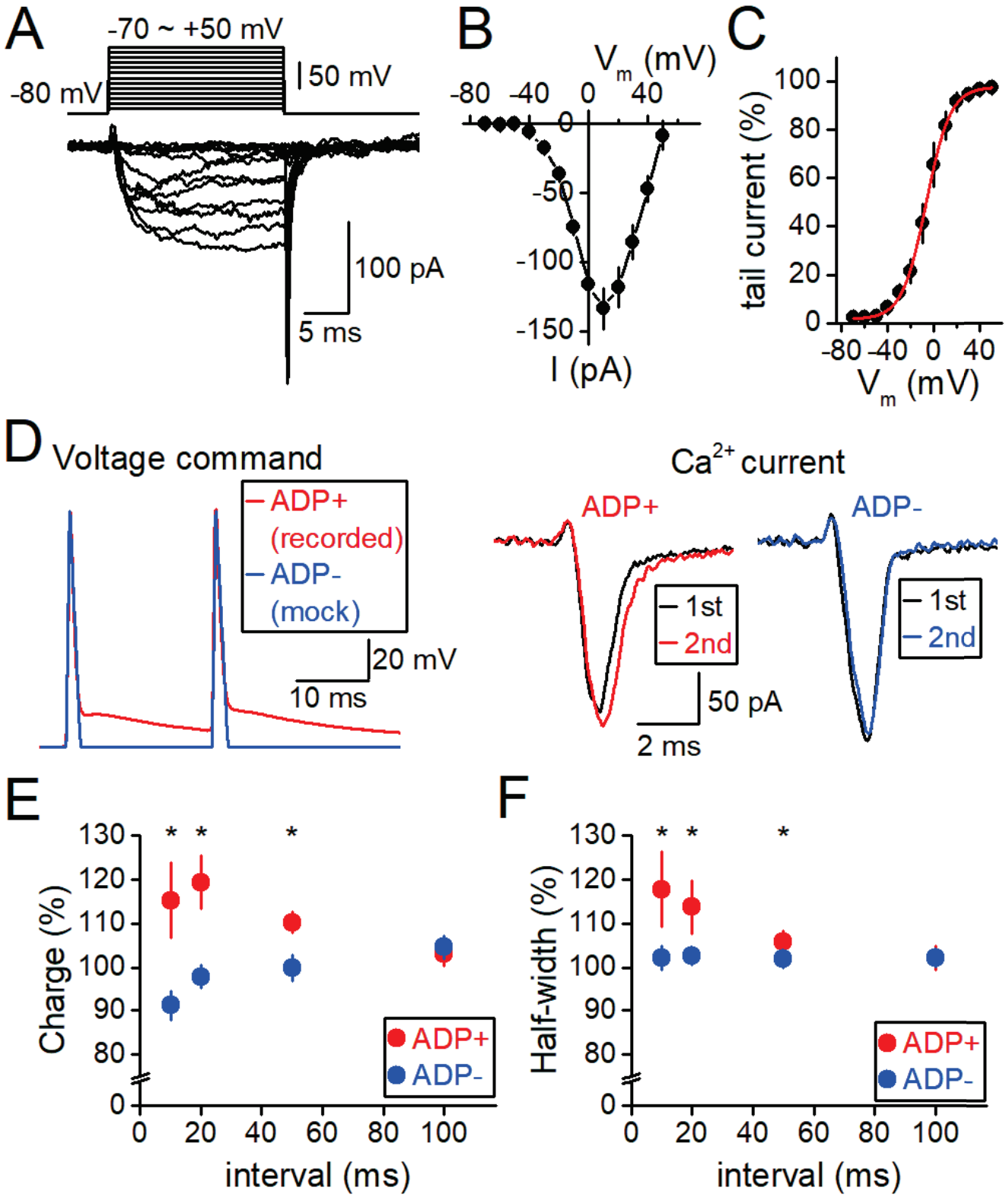
eNeuro Accepted Manuscript